AFRL-SN-WP-TP-2006-106

A TRANSIENT SPICE MODEL FOR DIELECTRIC-CHARGING EFFECTS IN RF MEMS CAPACITIVE SWITCHES (PREPRINT)

Xiaobin Yuan, James C.M. Hwang, David I. Forehand, and Charles L. Goldsmith

MARCH 2006

STINFO COPY

**SENSORS DIRECTORATE
AIR FORCE RESEARCH LABORATORY
AIR FORCE MATERIEL COMMAND
WRIGHT-PATTERSON AIR FORCE BASE, OH 45433-7320**

NOTICE AND SIGNATURE PAGE

Using Government drawings, specifications, or other data included in this document for any purpose other than Government procurement does not in any way obligate the U.S. Government. The fact that the Government formulated or supplied the drawings, specifications, or other data does not license the holder or any other person or corporation; or convey any rights or permission to manufacture, use, or sell any patented invention that may relate to them.

This report was cleared for public release by the Air Force Research Laboratory Wright Site (AFRL/WS) Public Affairs Office and is available to the general public, including foreign nationals. Copies may be obtained from the Defense Technical Information Center (DTIC) (http://www.dtic.mil).

AFRL-SN-WP-TP-2006-106 HAS BEEN REVIEWED AND IS APPROVED FOR PUBLICATION IN ACCORDANCE WITH ASSIGNED DISTRIBUTION STATEMENT.

//Signature//   //Signature//

JOHN L. EBEL   KENICHI NAKANO, Chief
Devices for Sensing Branch   Devices for Sensing Branch
Aerospace Components Division   Aerospace Components Division

//Signature//

TODD A. KASTLE, Chief
Aerospace Components Division
Sensors Directorate

This report is published in the interest of scientific and technical information exchange, and its publication does not constitute the Government's approval or disapproval of its ideas or findings.

REPORT DOCUMENTATION PAGE

Form Approved
OMB No. 0704-0188

1. REPORT DATE *(DD-MM-YY)*	2. REPORT TYPE	3. DATES COVERED *(From - To)*
March 2006	Journal Article Preprint	08/23/2003 – 03/01/2006

4. TITLE AND SUBTITLE
A TRANSIENT SPICE MODEL FOR DIELECTRIC-CHARGING EFFECTS IN RF MEMS CAPACITIVE SWITCHES (PREPRINT)

5a. CONTRACT NUMBER
F33615-03-C-7003

5b. GRANT NUMBER

5c. PROGRAM ELEMENT NUMBER
63739E

6. AUTHOR(S)
Xiaobin Yuan, James C.M. Hwang, David I. Forehand, and Charles L. Goldsmith

5d. PROJECT NUMBER
ARPS

5e. TASK NUMBER
ND

5f. WORK UNIT NUMBER
AN

7. PERFORMING ORGANIZATION NAME(S) AND ADDRESS(ES)

MEMtronics Corporation
3000 Custer Road, Suite 270-400
Plano, TX 75075

8. PERFORMING ORGANIZATION REPORT NUMBER

9. SPONSORING/MONITORING AGENCY NAME(S) AND ADDRESS(ES)

Sensors Directorate
Air Force Research Laboratory
Air Force Materiel Command
Wright-Patterson Air Force Base, OH 45433-7320

10. SPONSORING/MONITORING AGENCY ACRONYM(S)
AFRL-SN-WP

11. SPONSORING/MONITORING AGENCY REPORT NUMBER(S)
AFRL-SN-WP-TP-2006-106

12. DISTRIBUTION/AVAILABILITY STATEMENT
Approved for public release; distribution is unlimited.

13. SUPPLEMENTARY NOTES
PAO Case Number: AFRL/WS 06-0990, 17 Apr 2006.

This work has been submitted to IEEE for publication in *IEEE Transactions on Electron Devices*.

14. ABSTRACT

A transient SPICE model for dielectric-charging effects in RF MEMS capacitive switches was developed and implemented in a popular microwave circuit simulator. In this implementation the dielectric-charging effects are represented by RC sub-circuits with the sub-circuit parameters extracted from directly measured charging and discharging currents in the pA range. The resulted model was used to simulate the actuation-voltage shift in RF MEMS capacitive switches due to repeated operation and charging of the switch dielectric.

Agreement was obtained between the simulated and measured actuation-voltage shift under various control waveforms. For RF MEMS capacitive switches that fail mainly due to dielectric charging, the present SPICE model can be used to design control waveforms that can either prolong lifetime or accelerate failure.

15. SUBJECT TERMS
RF MEMS, Dielectric Charging, low loss

16. SECURITY CLASSIFICATION OF:			17. LIMITATION OF ABSTRACT:	18. NUMBER OF PAGES	19a. NAME OF RESPONSIBLE PERSON (Monitor)
a. REPORT Unclassified	**b. ABSTRACT** Unclassified	**c. THIS PAGE** Unclassified	SAR	14	John L. Ebel
					19b. TELEPHONE NUMBER *(Include Area Code)* N/A

Standard Form 298 (Rev. 8-98)
Prescribed by ANSI Std. Z39-18

i

A Transient SPICE Model for Dielectric-Charging Effects in RF MEMS Capacitive Switches

Xiaobin Yuan, *Student Member, IEEE*, Zhen Peng, *Student Member, IEEE*, James C. M. Hwang, *Fellow, IEEE*, David Forehand, *Member, IEEE*, and Charles L. Goldsmith, *Senior Member, IEEE*

Abstract—A transient SPICE model for dielectric-charging effects in RF MEMS capacitive switches was developed and implemented in a popular microwave circuit simulator. In this implementation the dielectric-charging effects are represented by *RC* sub-circuits with the sub-circuit parameters extracted from directly measured charging and discharging currents in the pA range. The resulted model was used to simulate the actuation-voltage shift in RF MEMS capacitive switches due to repeated operation and charging of the switch dielectric. Agreement was obtained between the simulated and measured actuation-voltage shift under various control waveforms. For RF MEMS capacitive switches that fail mainly due to dielectric charging, the present SPICE model can be used to design control waveforms that can either prolong lifetime or accelerate failure.

Index Terms—Charging, dielectric, lifetime, MEMS, RF, reliability, switch, SPICE, transient, trap, accelerated life test.

I. INTRODUCTION

IN the past decade, RF MEMS has emerged as a promising technology for low-loss switch, phase shifter, and reconfigurable network applications [1]-[4]. However, commercialization of RF MEMS devices is hindered by the need for continuing improvements in reliability and packaging. In particular, lifetime of electrostatically actuated RF MEMS capacitive switches is limited by dielectric-charging effects [5]. The dielectric is typically low-temperature deposited silicon dioxide or nitride with a high density (10^{18} cm^{-3}) of traps associated with silicon dangling bonds. During switch operation, the electric field across the dielectric can be higher than 10^6 V/cm causing charge carriers to be injected into the dielectric and become trapped. With repeated operation, charge gradually builds up in the dielectric, which modifies the electrostatic force on the movable membrane resulting in actuation-voltage shift [6].
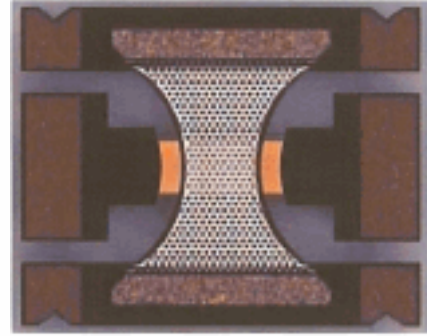
Dielectric-charging effects in RF MEMS have been

Fig. 1. Top view of a state-of-the-art RF MEMS capacitive switch.

researched by different groups [5]-[9] with a qualitative charging model proposed [9]. In comparison, we have proposed an equation-based quantitative charging model to predict charge injection and actuation-voltage shift [10]. In this paper we implement the equation-based model as equivalent circuit in a popular microwave circuit simulator ADS[1]. The equivalent-circuit model is then used in transient circuit simulation under various control waveforms. The results are in general agreement with that simulated by the equation-based model and the measured actuation-voltage shift. Therefore, for RF MEMS capacitive switches that fail mainly due to dielectric charging, the present model can be used to design control waveforms that can either prolong lifetime or accelerate failure. The present model complements existing equivalent-circuit models of MEMS switches, hence can be used to simulate the performance and reliability of circuits comprising multiple MEMS and electronic devices in the future.

II. MODEL EXTRACTION

Fig. 1 illustrates a state-of-the-art metal-dielectric-metal RF MEMS capacitive switch fabricated on a glass substrate. The dielectric is sputtered silicon dioxide with a thickness of 0.25 μm and a dielectric constant of 4.0. The top electrode is a 0.3-μm-thick flexible aluminum membrane that is grounded. The bottom chromium/gold electrode serves as the center conductor of a 50 Ω coplanar waveguide for the RF signal. Without any electrostatic force, the membrane is normally suspended in air 2.5 μm above the dielectric. Control voltage with a magnitude of 25-35 V is applied to the bottom electrode, which brings the membrane in contact with the dielectric thus

TABLE I
EXTRACTED MODEL PARAMETERS

	Positive Bias			
J	τ_C (s)	τ_D (s)	Q_0 (cm^{-2})	V_0 (V)
1	6.6	6.8	3.1×10^{10}	12.9
2	54.3	61.6	1.6×10^{11}	14.9
	Negative Bias			
J	τ_C (s)	τ_D (s)	Q_0 (cm^{-2})	V_0 (V)
1	6.5	7.0	2.4×10^{10}	11.7
2	52.5	74.7	6.0×10^{10}	10.5

forming a 120 μm x 80 μm capacitor to shunt the RF signal to ground. When the control voltage is reduced to below the release voltage of 8 V, the membrane springs back to its fully suspended position, resulting in little capacitive load to the RF signal. The switch has low insertion loss (0.06 dB) and reasonable isolation (15 dB) at 35 GHz. The switching time is less than 10 μs.

A charging model was constructed for the switch from the measured transient charging/discharging currents on the switch dielectric [10]. The injected charge density in the dielectric is modeled as

$$Q = \sum_J Q_J [1 - \exp(-t_{ON}/\tau_{CJ})]\exp(-t_{OFF}/\tau_{DJ}), \qquad (1)$$

where Q_J is the steady-state charge density of the Jth species of trap, τ_C and τ_D are the charging and discharging time constants, t_{ON} and t_{OFF} are the on and off times of the switch corresponding to the charging and discharging times.

Charging and discharging currents caused by the trapped charges are expressed as in the following:

$$I_c = qA\frac{dQ}{dt} = qA\sum_J \frac{Q_J}{\tau_{CJ}}\exp(-t_{ON}/\tau_{CJ}), \qquad (2)$$

$$I_D = qA\frac{dQ}{dt} = -qA\sum_J \frac{Q_J}{\tau_{DJ}}\exp(-t_{OFF}/\tau_{DJ}), \qquad (3)$$

where q is the electron charge and A is the surface area of the dielectric.

From the measured charging and discharging transient currents of the traps in the switch dielectric, model parameters Q_J, τ_{CJ}, and τ_{DJ} were extracted for different control voltages by fitting the measured data with exponential functions of (2) and (3). Two exponential functions, representing two trap species, were found to give good fit.

As shown in Fig. 2(a), the extracted charging and discharging time constants for both positive and negative control voltages exhibited little voltage dependence. Therefore, τ_C and τ_D were taken as the average value under different voltages. By contrast, the steady-state charge densities were found to vary exponentially with control voltage, as illustrated
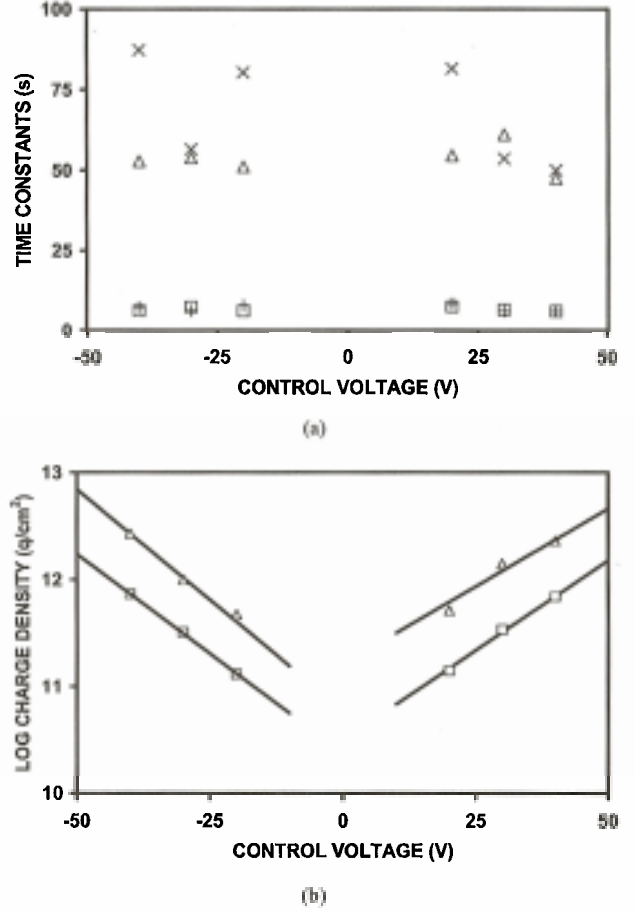

(a)

(b)

Fig. 2. (a) Trap 1 (□) charging and (+) discharging and trap 2 (Δ) charging and (x) discharging time constants. (b) Extracted (symbols) and fitted (lines) steady-state charge densities for (□) trap 1 and (Δ) trap 2 under -40, -30, -20, 20, 30, and 40 V. The time constants show no significant bias dependence whereas the steady-state charge densities are exponentially dependent on the control voltage.

in Fig. 2(b). Voltage dependence of the steady-state charge density for the Jth trap is therefore modeled as

$$Q_J = Q_{0J}\exp(V/V_{0J}), \qquad (4)$$

where V is the absolute value of control voltage, Q_0 and V_0 are fitting parameters. Using the above-described approach, two sets of model parameters were extracted for positive and negative control voltages, respectively, as listed in Table I.

The actuation-voltage shift due to dielectric charging can be expressed as

$$\Delta V = qhQ/\varepsilon_0\varepsilon_r, \qquad (5)$$

where h is the distance between the bottom electrode and the trapped charge sheet, Q is the injected charge density predicted by the charging model (1), ε_0 is the permittivity of free space, and ε_r is the relative dielectric constant. Approaches to
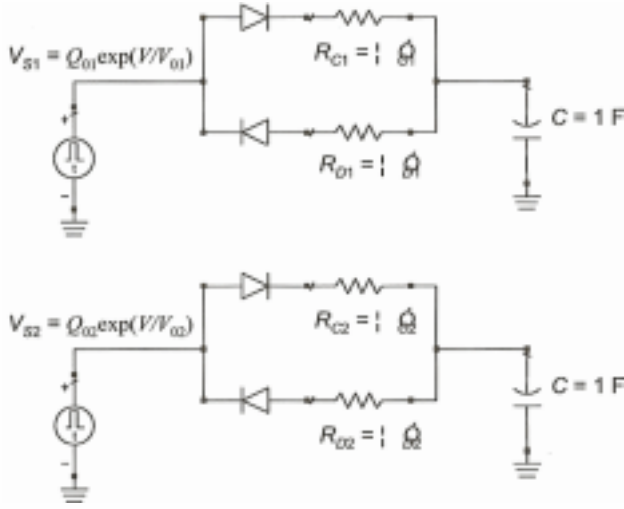
2

Fig. 3. ADS equivalent-circuit model for transient circuit simulation. Voltage dependence of the steady-state charge densities was implemented in the two voltage sources. Diodes were used to direct charge flow. $C = 1$ F, $R_{C1} = 6.5$ Ω, $R_{D1} = 7.0$ Ω, $R_{C2} = 52.5$ Ω, and $R_{D2} = 74.7$ Ω.

calculate Q under complex control waveforms will be presented in the following section. The injected charges are most likely distributed across the thickness of the dielectric. Since their collective effect on the actuation voltage can be approximated by a charge sheet, it greatly simplifies the model by using the charge-sheet assumption. Since h cannot be directly measured, actuation-voltage shift for a certain stress period is predicted by the charging model (1), (4), and (5) with an optimized h value to give the best fit between model prediction and experimental data under all control waveforms.

III. MODEL IMPLEMENTATION

A. Equivalent-Circuit Model

In order to calculate charge injection under complex control waveforms, the extracted charging model was implemented into ADS using an approach similar to that in [11]. As shown in Fig. 3, two RC sub-circuits were used to simulate charging and discharging of two trap species. Both capacitances were set to unity so that the resistance values represent different time constants: $R_{C1} = \tau_{C1}$, $R_{C2} = \tau_{C2}$, $R_{D1} = \tau_{D1}$, and $R_{D2} = \tau_{D2}$. Diodes in the sub-circuits were used to direct charge flow. Therefore, the capacitor is charged through R_C during the switch on time when the source voltage is greater than the capacitor voltage. Similarly, the capacitor discharges through R_D during the off time when the source voltage is smaller than the capacitor voltage. Total charge accumulated on the unity capacitances represents total trapped charge in the switch dielectric. Voltage dependence of the steady-state charge densities in (4) was implemented into the two voltage sources. Therefore, after defining the time-domain switch control waveform in the
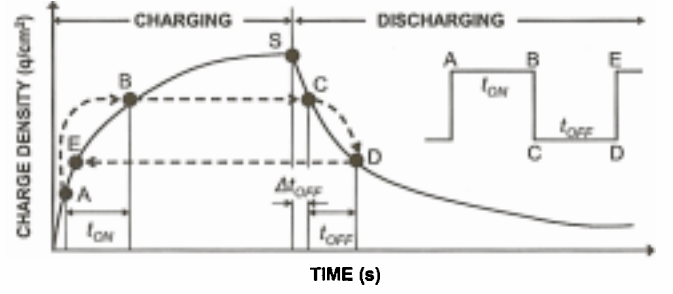

Fig. 4. Charging calculation under a square wave using the equation-based model. t_{ON} and t_{OFF} are the on and off times of the switch. After one operating cycle, charge density increases from the initial state A to the end state E. Inset illustrates the applied square wave and the corresponding charging states.

voltage sources, charge injection and actuation-voltage shift can be simulated using transient circuit simulation.

B. Equation-Based Model

Another modeling approach was used to calculate charge injection under square-wave actuation. This is referred to as the equation-based model in contrast to the above-described equivalent-circuit model. Fig. 4 illustrates a charging curve that starts from the origin and ends in saturation (state S), which is followed by a discharging curve that falls exponentially as shown in the charging model (1). The charging and discharging curves shown in Fig. 4 are generated from the charging model equations and can be expressed as in the following:

$$Q = \sum_J Q_J [1 - \exp(-t_{ON}/\tau_{CJ})], \tag{6}$$

$$Q = \sum_J Q_J \exp(-t_{OFF}/\tau_{DJ}), \tag{7}$$

where Q_J is the voltage-dependent steady-state charge density of the Jth species of trap, τ_{CJ} and τ_{DJ} are the corresponding charging and discharging time constants.

During real switch operation under a square wave, the charging state at the beginning of each operating cycle can be somewhere between empty and full, such as state A illustrated on the charging curve. After the switch is turned on, the charging state moves higher to state B during the on time of the switch. After the switch is turned off, the dielectric starts to discharge from state C on the discharging curve, which is mapped horizontally from state B of the charging curve. After certain off time, the dielectric is discharged to state D, which is then mapped back to state E on the charging curve to start the next operating cycle. Thus, the net effect of one operating cycle of the switch is to move the charging state from A to E. This equation-based charging/discharging model repeats in such a ratchet fashion until the desired number of cycles has been operated. To calculate charge injection under square waves, the model needs four input parameters: peak voltage, on time, off time, and number of cycles. Alternatively, on and off times can be specified in terms of frequency and duty factor of the waveform.

3

IV. COMPARISON WITH MEASURED RESULTS

A. Accelerated Test Setup

Accelerated life tests for the switch shown in Fig. 1 were performed on a time-domain switch characterization setup [6]. A 6 GHz, 10 dBm sinusoidal signal was applied to the switch input port together with the control waveform. RF output was sensed by using a Narda 26.5 GHz diode detector. Both the control and output waveforms were monitored by using an oscilloscope. First, a 0 to −30 V saw-tooth control wave was applied to the bottom electrode of a pristine switch to sense the pre-stress actuation voltage. Next, the switch was stressed by applying a square or dual-pulse wave for different stress periods. After each stress period, another saw-tooth control wave was applied to the switch to sense the post-stress actuation voltage. This way, the actuation-voltage shift for each stress period can be determined. Different stress waveforms were used to drive the switch in order to study the acceleration factors of the charging effects. Specifically, square waves with different peak voltages, duty factors, and frequencies were used, so were dual-pulse waveforms with different pull-down pulse widths.

B. Square-Wave Actuation

Under a square control wave, the amount of charging within one operating cycle is determined by three parameters: peak voltage, duty factor, and frequency. We first investigate the effects of frequency and duty factor, while keeping the peak voltage constant. Specifically, the square wave used in the study has an on voltage of −30 V and an off voltage of 0. The actuation voltage of the pristine switch is approximately −22 V at room temperature. Therefore, peak voltage of −30 V ensures switch operation after significant actuation-voltage shift in either direction. A pristine switch was operated at two different frequencies: 10 and 100 Hz. Three duty factors were used at each frequency: 25%, 50%, and 75%.

After stressing the switch with the 0 to −30 V square wave for a certain period, actuation voltage was shifted in the positive direction (less negative) indicating injection of electrons from the bottom electrode into the dielectric. Agreement was found between simulated and measured actuation-voltage shifts at both frequencies as shown in Fig. 5. Simulation results from both equivalent-circuit and equation-based models are presented. Difference between the two modeling approaches will be discussed at the end of this section. Both simulated and measured data suggest that for a fixed duty factor, dielectric charging and actuation-voltage shift depend strongly on the total stress time instead of number of operating cycles. Notice that for both frequencies, actuation-voltage shifts for the same stress period are almost identical. So long as the stress frequency is much greater than the inverse of charging/discharging time constants, charge injection has no obvious dependence on the stress frequency. This is consistent with the experimental results in [9]. On the other hand, increasing the duty factor accelerates dielectric charging and actuation-voltage shift at both frequencies as
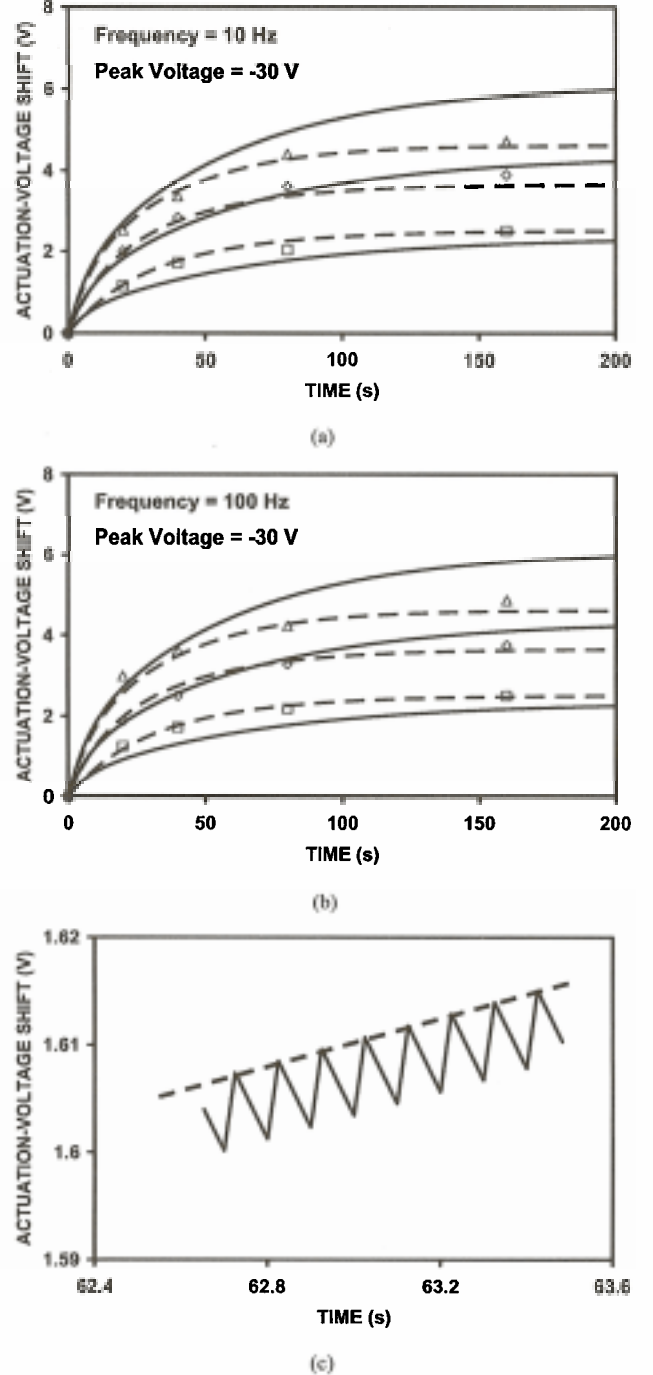

(a)

(b)

(c)

Fig. 5. Actuation-voltage shift as a function of stress time and frequency. The stress signal is a 0 to −30 V square wave at (a) 10 and (b) 100 Hz. Actuation-voltage shifts are simulated using (—) equivalent-circuit and (---) equation-based models with 25%, 50%, and 75% duty factors bottom up. Measured actuation-voltage shifts are for (□) 25%, (◊) 50%, and (Δ) 75% duty factors. (c) Detailed view of the 25% duty factor trace in (a) simulated by the equivalent-circuit model showing the charging and discharging dynamics of the traps. Dashed line represents the envelope of the charging/discharging transient. Both simulated and measured data show that, giving the present test conditions, actuation-voltage shift is accelerated by duty factor, but not by frequency.

4

shown in Fig. 5. Fig. 5(c) shows a detailed view of the ADS simulated actuation-voltage shift, which increases in a saw-tooth fashion through charging and discharging of the traps within each operating cycle.

For a giving frequency, the charging and discharging times within one operating cycle are determined by the duty factor. For the extreme case of dc stress (duty factor = 100%), the charge density will eventually reach a saturated value $\sum Q_J$, which is implemented in the voltage sources using (4). For an extremely low duty factor such as 0.01%, the charge accumulated during the on time of the switch will be discharged almost completely during the off time; hence little charge will ever be accumulated. An intermediate duty factor, e.g., 50%, will cause the charge density to saturate at a value somewhere between 0 and $\sum Q_J$ when the charging and discharging processes are balanced. In a pristine switch, charging is fast to start with while discharging is slow. This builds up charge so that charging slows down while discharging accelerates until charging and discharging are balanced. With the proper switch design and control waveform, it is possible to avoid switch failure even after charging or actuation-voltage shift saturates. Therefore, the commonly quoted number of cycles before failure, due to its dependence on the detailed actuation waveform, is not a universal figure of merit for RF MEMS capacitive switches [9]. For a square control wave with a peak voltage that is defined by the actuation voltage, frequency and duty factor must be specified for the quoted life cycles to be meaningful. Conversely, with the acceleration effects quantified through the present charging model, a fair comparison can be made between lifetimes measured under different frequencies and duty factors.

Empirically it has been reported that the switch lifetime depends on the total on time and not on duty factor or frequency of the control waveform. Our results in Fig. 5 also show that charging has no obvious dependence on stress frequency. Using the present model we show in the following analysis that this is only the limiting case when the switching period is much shorter than charging/discharging time constants and the total accumulated charge is much smaller than the saturated (steady-state) charge.

Considering the RC sub-circuits in Fig. 3, during the on time of an operating cycle, the capacitor is charged through R_C, the voltage accumulated on the capacitor after the on time is

$$V(t+t_{ON}) = V_s[1 - \exp(-t_{ON}/\tau_C)] + V(t)\exp(-t_{ON}/\tau_C), \quad (8)$$

where V_S is the source voltage and $V(t)$ is the initial voltage on the capacitor before the on time starts. For now we assume that there is only one species of traps so the subscript "J" can be dropped. During the off time of the operating cycle, the capacitance is discharged through R_D, the voltage/charge left on the capacitor at the end of the off time is

$$V(t+t_{ON}+t_{OFF}) = V(t+t_{ON})\exp(-t_{OFF}/\tau_D). \quad (9)$$

Thus, (8) and (9) can be used repeatedly to evaluate the charging state after ensuing operation cycles.

If $t_{ON} \ll \tau_C$ and $t_{OFF} \ll \tau_D$, (8) and (9) reduce to

$$V(t+t_{ON}) \cong V_s \cdot t_{ON}/\tau_C + V(t)(1 - t_{ON}/\tau_C); \quad (10)$$

$$V(t+t_{ON}+t_{OFF}) \cong V(t+t_{ON})(1 - t_{OFF}/\tau_D). \quad (11)$$

Assuming a pristine capacitor without any charge at $t = 0$, after the on time of the first operating cycle, the accumulated voltage given by (10) is

$$V(t_{ON}) \cong (V_s \cdot t_{ON}/\tau_C). \quad (12)$$

The voltage left on the capacitor after the ensuing off time is given by (11) as

$$V(t_{ON}+t_{OFF}) \cong (V_s \cdot t_{ON}/\tau_C)(1 - t_{OFF}/\tau_D). \quad (13)$$

Following the same procedure, charge accumulation after the second on time is expressed as

$$V(2 \cdot t_{ON}+t_{OFF}) \cong (V_s \cdot t_{ON}/\tau_C) \cdot [1 + (1 - t_{ON}/\tau_C)(1 - t_{OFF}/\tau_D)]. \quad (14)$$

Hence, charge accumulation after the *nth* on time is expressed as

$$V[n \cdot t_{ON}+(n-1)t_{OFF}] \cong (V_s \cdot t_{ON}/\tau_C) \cdot \sum_{m=1}[(1 - t_{ON}/\tau_C)(1 - t_{OFF}/\tau_D)]^{m-1}. \quad (15)$$

After Taylor Series expansion and dropping higher order terms, (15) reduces to

$$V[n \cdot t_{ON}+(n-1)t_{OFF}] \cong (V_s \cdot t_{ON}/\tau_C) \cdot \sum_{m=1}[1 - (m-1)(t_{ON}/\tau_C + t_{OFF}/\tau_D)]. \quad (16)$$

After summing the arithmetical progression in (16) and dropping insignificant terms, (16) is reduced to

$$V[n \cdot t_{ON}+(n-1)t_{OFF}]$$
$$\cong \frac{V_s(n \cdot t_{ON})}{\tau_C}[1 - \frac{1}{2} \cdot (\frac{n \cdot t_{ON}}{\tau_C} + \frac{n \cdot t_{OFF}}{\tau_D})]$$
$$\cong \frac{V_s(T \cdot P)}{\tau_C}\{1 - \frac{1}{2} \cdot [\frac{T \cdot P}{\tau_C} + \frac{T \cdot (1-P)}{\tau_D}]\}, \quad (17)$$

where $T = n(t_{ON} + t_{OFF})$ is the total stress time and $P = t_{ON}/(t_{ON} + t_{OFF})$ is the duty factor. Therefore, when the frequency is high so that $t_{ON} \ll \tau_C$ and $t_{OFF} \ll \tau_D$, charge injection is only affected by total stress time and duty factor, but not by
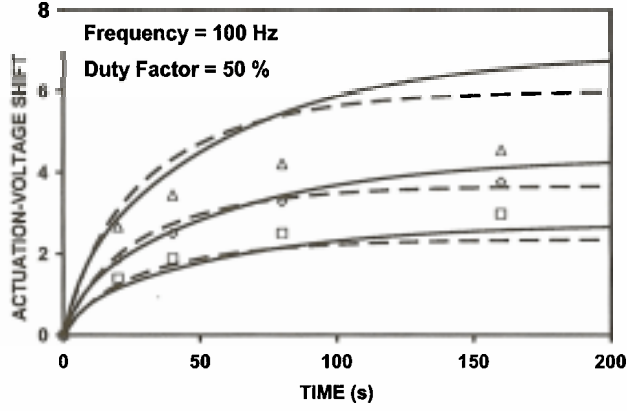
5

Fig. 6. Actuation-voltage shift as a function of stress time and peak voltage under a 100 Hz, 50% duty factor square wave. Actuation-voltage shifts are simulated using (—) equivalent-circuit and (---) equation-based models with −25 V, −30 V, and −35 V peak voltages bottom up. Measured actuation-voltage shifts are for (□) −25 V, (◊) −30 V, and (Δ) −35 V peak voltages. Both simulated and measured data show that charge injection is accelerated by increasing the peak voltage.

Fig. 7. Simulated charge density during the off time after a −30 V, 50 ms on time using the (—) equivalent-circuit model and (---) equation-based model.

frequency. In addition to the assumption of $t_{ON} \ll \tau_C$ and $t_{OFF} \ll \tau_D$, if we also assume that $n \cdot (t_{ON}/\tau_C + t_{OFF}/\tau_D) \ll 1$, (17) reduces to

$$V(T) = V_s (T \cdot P)/\tau_c, \tag{18}$$

where $T \cdot P$ is the total on time. Therefore, when the switching period is much shorter than charging/discharging time constants and the total number of operated cycles is small so that accumulated charge is much smaller than the saturated (steady-state) charge, trapped charge is proportional to the total switch on time as has been observed.

It has been shown that increasing the peak voltage accelerates charge injection and shortens the switch lifetime [5]. Voltage acceleration of dielectric charging was studied using a 100 Hz, 50% duty factor square wave with −25 V, −30 V, and −35 V peak voltages. Both simulated and measured data in Fig. 6 confirm that increasing the peak voltage accelerates dielectric charging resulting in larger actuation-voltage shifts at higher voltages. Since peak voltage affects steady-state charge densities but not charging/discharging time constants (Fig. 2), similar voltage acceleration can be expected for other frequencies and duty factors.

As shown by the measured and simulated results in Fig. 5 and 6, both equivalent-circuit and equation-based models predict that dielectric charging is accelerated by duty factor and peak voltage instead of operating frequency of the control waveform. However, when there are more than one species of traps with different time constants involved, there can be subtle differences between the two modeling approaches causing the simulated results from the two models to be slightly different. To examine such differences, we need to sum over the subscript
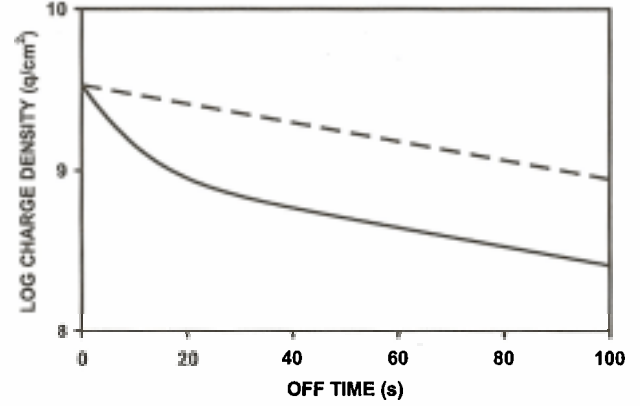
"J." Considering a pristine switch without trapped charge, after the first on time, the amount of trapped charge is determined by

$$V(t_{on}) = \sum_J V_{SJ}[1 - \exp(-t_{on}/\tau_{CJ})] \tag{19}$$

for both models. The charge after the ensuing off time is predicted by the equivalent-circuit model as

$$V(t_{on} + t_{off}) = \sum_J V_{SJ}[1 - \exp(-t_{on}/\tau_{CJ})]\exp(-t_{off}/\tau_{DJ}). \tag{20}$$

On the other hand, by using the calculation routine illustrated in Fig. 4, the amount of charge during the ensuing off time is predicted by the equation-based model as

$$V'(t_{on} + t_{off}) = \sum_J V_{SJ} \exp[-(t_{off} + \Delta t_{off})/\tau_{DJ}], \tag{21}$$

where the prime on V' indicates that it is calculated by the equation-based model. Δt_{OFF} is the time it takes for a full charge of ΣV_{SJ} to discharge to $V(t_{ON})$ as illustrated in Fig. 4. Therefore, we have $V'(t_{ON}) = \Sigma V_{SJ} \exp(-\Delta t_{OFF}/\tau_{DJ}) = V(t_{ON})$. This shows that both models predict same amount of charge at $t_{OFF} = 0$. In contrast, the discharging rates for the two models are different. In other words, derivatives of (20) and (21) are different resulting in the difference between simulation results generated by the two models. The derivatives of (20) and (21) at $t_{OFF} = 0$ can be expressed as

$$\frac{d[V(t_{on} + t_{off})]}{dt_{off}} = -\sum_J \frac{V_{SJ}[1 - \exp(-t_{on}/\tau_{CJ})]}{\tau_{DJ}}, \tag{22}$$

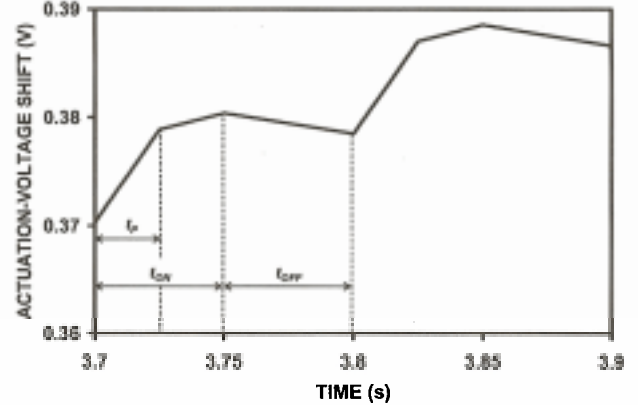$$\frac{d[V'(t_{on} + t_{off})]}{dt_{off}} = -\sum_J \frac{V_{SJ} \exp(-\Delta t_{off}/\tau_D)}{\tau_{DJ}}, \tag{23}$$
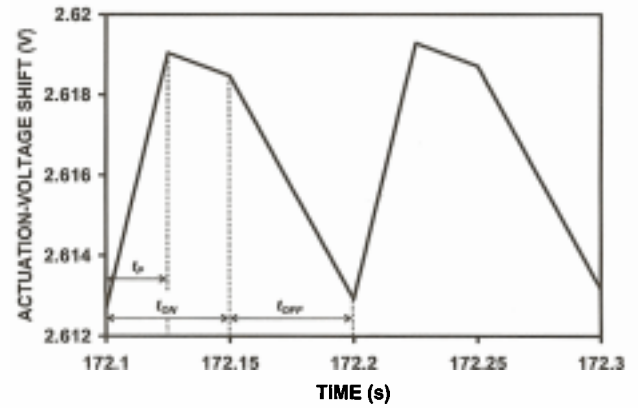
6
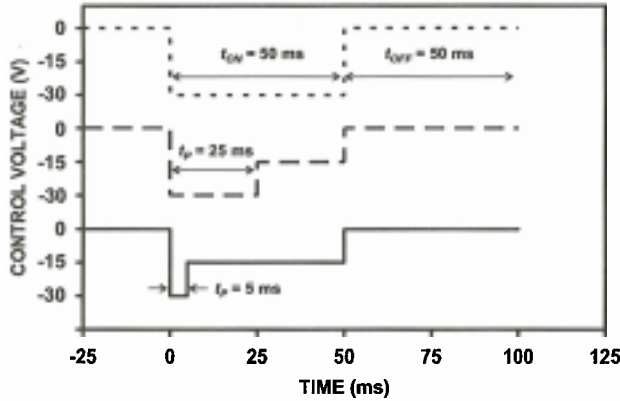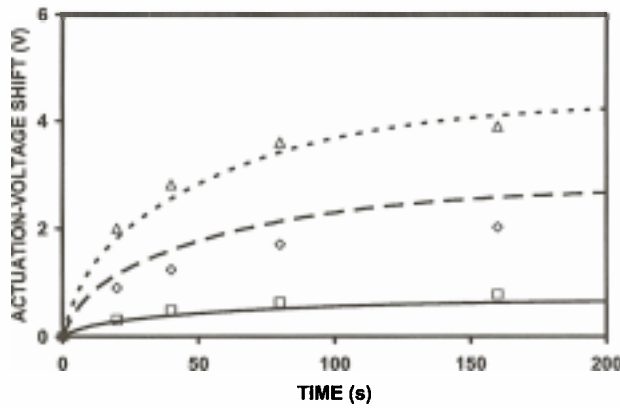
Fig. 8. (a) Illustration of (—) dual pulse with t_P = 5 ms, (---) dual pulse with t_P = 25 ms, and (···) 0 to −30 V square wave. The stress waveform frequency is 10 Hz. Both square and dual-pulse waves have 50% duty factor. For the dual-pulse waves, pull-down voltage is −30 V and hold-down voltage is −15 V. (b) Actuation-voltage shift as a function of stress time. ADS simulated actuation-voltage shifts are for (—) dual pulse with t_P = 5 ms, (---) dual pulse with t_P = 25 ms, and (···) 0 to −30 V square wave. Measured actuation-voltage shifts are for (□) dual pulse with t_P = 5 ms, (◊) dual pulse with t_P = 25 ms, and (△) 0 to −30 V square wave. Charge injection is minimized by using the dual-pulse waves instead of the square wave.

Fig. 9. ADS Simulated actuation-voltage shift as a function of stress time under a 10 Hz, 50% duty factor dual pulse with t_P = 25 ms. The pull-down voltage is −30 V and hold-down voltage is −15 V. (a) At the early stage of the stress period, charge is injected for the entire on time, resulting in continuous increasing of the actuation-voltage shift during the on time. (b) After the injected charge density exceeds the steady-state charge density defined by the hold-down voltage, traps start to discharge for the hold-down period of the on time resulting in decreasing of the actuation-voltage shift during the period.

Fig. 7 shows the comparison of the trapped charge during switch off time predicted by the two models indicating the difference between (22) and (23). Although both models start with the same amount of charge, the equation-based model has a smaller discharging rate and shows a more gradual decrease than the equivalent-circuit model. This causes more aggressive charge accumulation using the equation-based model. As a result, Fig. 6 shows that, trapped charge calculated by using the equation-based model will start with a sharper increase and will saturate sooner than that simulated by using the equivalent-circuit model. The difference between the two discharging traces in Fig. 7 will diminish as the on time before discharging increases. For extremely long on times (e.g., 500 s), traps are all charged to their steady-state values before the

off time starts so that $\Delta t_{OFF} = \exp(-t_{ON}/\tau_C) = 0$ and (20) and (21) become the same. In addition, if there is only one set of charging and discharging time constants representing one trap species, (22) and (23) are essentially the same, and so are (20) and (21). However, when a more complicated control waveform is involved in the analysis, the calculation routine using the equation-based model is not as straight forward as the square-wave case. Therefore, the equivalent-circuit model will be advantageous when analyzing dielectric charging under complex control waveforms (e.g., dual-pulse waveforms in the next section).

C. Dual-Pulse Actuation

A dual-pulse waveform has been proposed to minimize charging [5]. The waveform comprises a short high-voltage pulse to quickly pull down the membrane and a low-voltage

7

pulse to hold down the membrane for the remaining on time. Thus, for most of the on time the dielectric is subject to the low-voltage hold-down pulse and charging is minimized due to its exponential voltage dependence. As illustrated in Fig. 8(a), the dual pulse used in our measurement and simulation is a 10 Hz, 50% duty factor ($t_{ON} = t_{OFF} = 50$ ms) signal. The pull-down voltage is -30 V and the hold-down voltage is -15 V. The pull-down pulse width (t_P) was varied as a parameter. Comparing with a 0 to -30 V square wave, the dual-pulse waveforms minimized dielectric charging as expected. The present model can correctly predict the charging trend under such dual-pulse waveforms as shown in Fig. 8(b).

Detailed charging/discharging dynamics for the dual-pulse waveforms are more complicated than the square wave case shown in Fig. 5(c). The pull-down and hold-down voltages correspond to two steady-state charge densities predicted by (4). For the dual-pulse waveform shown in Fig. 8(a) with $t_P = 25$ ms, detailed trap charging/discharging dynamics after different stress periods are shown in Fig. 9. At the beginning of the dual-pulse stress, the trapped charge starts with a sharp increase under the -30 V pull-down pulse, followed by a gradual increase for the rest of the on time under the -15 V hold-down pulse, then decreases during the off time as shown in Fig. 9(a). As the trapped charge builds up in the dielectric and exceeds the steady-state charge density defined by the hold-down voltage, the hold-down pulse is no longer able to inject charge into the dielectric. Therefore, the traps will discharge under the hold-down pulse causing the actuation-voltage shift to decrease during the hold-down period as shown in Fig. 9(b). The above-described dynamics is determined by the shape of the specific dual-pulse waveform (i.e., pull-down voltage and pulse width, hold-down voltage and pulse width, on and off times).

V. Discussion

Transient circuit simulation using the equivalent-circuit model in Fig. 3 can take hours to converge for high frequency control waveforms (e.g., 10 KHz). This is caused by the fact that the simulator will try to capture the full transient response (saw-tooth like charging/discharging dynamics as illustrated in Fig. 5(c) and Fig. 9) of the RC circuits with long settling times. Using (8) and (9), charge injection under square waves for certain stress period can be calculated iteratively. Within each operating cycle, injected charge can be calculated at the end of the on time resulting in an envelope of the charging/discharging transient shown in Fig. 5(c). Thus, for high frequency square waves, this iterative calculation routine is a much more efficient alternative to the transient circuit simulation in that it is capable of obtaining the envelope of the transient without having to capture the charging/discharging details within each operating cycle. However, when a more complex control waveform is used to drive the switch, theoretical analysis can be much more involved than the square-wave case making the circuit simulation favorable.

For RF MEMS capacitive switches whose lifetime is limited by dielectric charging, the present analysis shows that the number of operating cycles before failure is not a universal figure of merit. As shown in (17), as long as the stress frequency is much greater than the inverse of charging/discharging time constants, charge injection is determined by the total stress time and duty factor instead of stress frequency or number of cycles. Peak voltage is also a critical acceleration factor as shown in (4). These acceleration effects are experimentally verified and compared with simulated results as shown in Fig. 5 and 6. Therefore, control waveforms with high peak voltage, high duty factor, and low frequency can be used to accelerate failure. Conversely, control waveforms of low peak voltage, high frequency, and low duty factor may retard failure and result in improved lifetimes. In general, peak voltage, frequency, and duty factor must be specified to allow fair comparison of switch lifetimes.

VI. Conclusion

A transient SPICE model for dielectric-charging effects in RF MEMS capacitive switches was developed and implemented in a commercially available circuit simulator ADS. The model was used to analyze charge injection under different control waveforms and was found to be in agreement with experimental data. Both simulated and measured data show that, dielectric-charging effects can be accelerated through duty factor and peak voltage of the control waveform whereas frequency is not an acceleration factor. Therefore, for RF MEMS capacitive switches that fail mainly due to dielectric charging, the present model can be used to analyze and design control waveforms that can either prolong lifetime or accelerate failure. This transient SPICE model also makes it convenient to simulate circuits that comprise multiple MEMS and electronic devices in the future.

References

[1] C. L. Goldsmith, Z. Yao, S. Eshelman, and D. Denniston, "Performance of low-loss RF MEMS capacitive switches," *IEEE Microwave Guided Wave Lett.,* vol. 8, pp. 269-271, Aug. 1998.

[2] D. Peroulis, S. Pacheco, K. Sarabandi, and L. P. B. Katehi, "MEMS devices for high isolation switching and tunable filtering," in *IEEE MTT-S Int. Microwave Symp. Dig.,* vol. 2, June 2000, pp. 1217-1220.

[3] A. Malczewski, S. Eshelman, B. Pillans, J. Ehmke, and C. L. Goldsmith, "X-band RF MEMS phase shifters for phased array applications," *IEEE Microwave Guided Wave Lett.,* vol. 9, pp. 517-519, Dec. 1999.

[4] G. M. Rebeiz, G.-L. Tan, and J. S. Hayden, "RF-MEMS phase shifters: design and applications," *IEEE Microwave Mag.,* vol. 3, pp. 72-81, June 2002.

[5] C. L. Goldsmith, J. Ehmke, A. Malczewski, B. Pillans, S. Eshelman, Z. Yao, J. Brank, and M. Eberly, "Lifetime characterization of capacitive RF MEMS switches," in *IEEE MTT-S Int. Microwave Symp. Dig.,* vol. 1, June 2001, pp. 227-230.

[6] X. Yuan, S. V. Cherepko, J. C. M. Hwang, C. L. Goldsmith, C. Nordquist, and C. Dyck, "Initial observation and analysis of dielectric-charging effects on RF MEMS capacitive switches," in *IEEE MTT-S Int. Microwave Symp. Dig.,* vol. 3, June 2004, pp. 1943-1946.

[7] W. M. van Spengen, R. Puers, R. Mertens, and I. De Wolf, "Experimental characterization of stiction due to charging in RF MEMS," *in IEDM Tech. Dig.,* Dec. 2002, pp. 901-904.

[8] J. R. Reid and R. T. Webster, "Measurements of charging in capacitive microelectromechanical switches," *Electron. Lett.,* vol. 38, no. 24, pp. 1544-1545, Nov. 2002.

[9] W. M. van Spengen, R. Puers, R. Mertens, and I. De Wolf, "A comprehensive model to predict the charging and reliability of capacitive RF MEMS switches," *J. Micromech. Microeng.*, vol. 14, no. 4, pp. 514-521, Jan. 2004.

[10] X. Yuan, J. C. M. Hwang, D. Forehand, and C. L. Goldsmith, "Modeling and characterization of dielectric-charging effects in RF MEMS capacitive switches," in *IEEE MTT-S Int. Microwave Symp. Dig.,* June 2005, pp. 753-756

[11] R. E. Leoni, III, M. S. Shirokov, J. W. Bao, and J. C. M. Hwang, "A phenomenologically based transient SPICE model for digitally modulated RF performance characteristics of GaAs MESFETs," *IEEE Trans. Microwave Theory Tech.,* vol. 49, no. 6, pp. 1180-1186, June 2001.